

THE END OF THE REIONIZATION EPOCH PROBED BY LY α EMITTERS AT $Z = 6.5$ IN THE SUBARU DEEP FIELD^{1,2}

NOBUNARI KASHIKAWA^{3,4}, KAZUHIRO SHIMASAKU^{5,6}, MATTHEW A. MALKAN⁷, MAMORU DOI⁸, YUICHI MATSUDA⁹,
 MASAMI OUCHI¹⁰, YOSHIAKI TANIGUCHI¹¹, CHUN LY⁷, TOHRU NAGAO^{3,12}, MASANORI IYE^{3,4},
 KENTARO MOTOHARA⁸, TAKASHI MURAYAMA¹¹, KOUJI MUROZONO⁵, KYOJI NARIAI¹³, KOUJI OHTA⁹,
 SADANORI OKAMURA^{5,6}, TOSHIYUKI SASAKI¹⁴, YASUHIRO SHIOYA¹¹, AND MASAYUKI UMEMURA¹⁵

Revised version after referee's report

ABSTRACT

We report an extensive search for Lyman α emitters (LAEs) at $z = 6.5$ in the Subaru Deep Field. Subsequent spectroscopy with Subaru/Keck identified eight more LAEs, giving us a total of 17 spectroscopically confirmed LAEs at $z = 6.5$. Based on these 17 spectroscopic sample complemented by the 58 photometric sample, we derived a more accurate Ly α luminosity function of LAEs at $z = 6.5$, that reveals an apparent deficit at the bright end, of ~ 0.75 mag fainter L^* , compared with that of $z = 5.7$. The difference of LAE luminosity functions between $z = 5.7$ and $z = 6.5$ has a 3σ significance, which is reduced to 2σ when taking into account the cosmic variance. This result could be an implication that the reionization of the universe has not been completed at $z = 6.5$. The spatial distribution of LAEs at $z = 6.5$ was found to be homogeneous over the field. We discuss some implications to the reionization of the universe.

Subject headings: cosmology: observation — early universe — galaxies: high-redshift — galaxies: formation

1. INTRODUCTION

The cosmic reionization is undoubtedly one of the major historical turning points of the early universe. The measurements of cosmic microwave background (CMB) temperature polarization by *Wilkinson Microwave Anisotropy Probe* (WMAP) implies an early reionization at $z = 10.9^{+2.7}_{-2.3}$ (Page et al. 2006), and

Electronic address: kashik@zone.mtk.nao.ac.jp

¹ The data presented herein were partly obtained at the W.M. Keck Observatory, which is operated as a scientific partnership among the California Institute of Technology, the University of California and the National Aeronautics and Space Administration. The Observatory was made possible by the generous financial support of the W.M. Keck Foundation.

² Based in part on the data collected at the Subaru Telescope, which is operated by the National Astronomical Observatory of Japan.

³ Optical and Infrared Astronomy Division, National Astronomical Observatory, Mitaka, Tokyo 181-8588, Japan.

⁴ Department of Astronomy, School of Science, Graduate University for Advanced Studies, Mitaka, Tokyo 181-8588, Japan.

⁵ Department of Astronomy, University of Tokyo, Hongo, Tokyo 113-0033, Japan.

⁶ Research Center for the Early Universe, University of Tokyo, Hongo, Tokyo 113-0033, Japan.

⁷ Department of Physics and Astronomy, University of California, Los Angeles, CA 90095-1547.

⁸ Institute of Astronomy, University of Tokyo, Mitaka, Tokyo 181-8588, Japan.

⁹ Department of Astronomy, Graduate School of Science, Kyoto University, Kyoto 606-8502, Japan.

¹⁰ Space Telescope Science Institute, 3700, San Martin Drive, Baltimore, MD 21218.

¹¹ Astronomical Institute, Graduate School of Science, Tohoku University, Aramaki, Aoba, Sendai 980-8578, Japan.

¹² INAF — Osservatorio Astrofisico di Arcetri, Largo Enrico Fermi 5, 50125 Firenze, Italy.

¹³ Department of Physics, Meisei University, 2-1-1 Hodokubo, Hino, Tokyo 191-8506, Japan.

¹⁴ Subaru Telescope, National Astronomical Observatory of Japan, 650 North A'ohoku Place, Hilo, HI 96720.

¹⁵ Center for Computational Physics, University of Tsukuba, 1-1-1 Tennodai, Tsukuba 305-8571, Japan.

the complete Gunn-Peterson trough of Sloan Digital Sky Survey (SDSS) QSOs suggests that cosmic reionization ended at $z \sim 6$ (Fan et al. 2002). There are disputes over when and how the reionization has taken place, and what objects are responsible for it. Although QSOs would be the main contributor of ionizing photons at the bright end of the luminosity function (LF) of ionizing sources, the QSO population alone cannot account for the entire required ionizing photons (Willott et al. 2005), and star-forming galaxies like Lyman break galaxies (LBGs) and Lyman α emitters (LAEs) at the reionization epoch would be the only alternatives that dominate at the faint end. The census of observable galaxies at this epoch is sensitive to the ionization fraction of the universe (Yan & Windhorst 2004; Malhotra & Rhoads 2004; Bouwens et al. 2005; Stiavelli et al. 2005; Bunker et al. 2006). It is expected that the surrounding neutral inter galactic medium (IGM) attenuates the Lyman α photons so significantly that the number density decline of LAEs provides a useful observational constraint on the reionization epoch (Haiman & Spaans 1999; Rhoads & Malhotra 2001; Hu et al. 2002).

There have been great advances over three years in detecting distant galaxies at the edge of the cosmic reionization era beyond $z = 6$ in both the dropout searches (Dickinson et al. 2004; Bouwens et al. 2003, 2005; Kneib et al. 2004; Pelló et al. 2004; Stanway, McMahon & Bunker 2005) to find their strong Lyman breaks and narrow-band (NB) searches (Hu et al. 2002; Cuby et al. 2003; Ajiki et al. 2003; Kodaira et al. 2003; Rhoads et al. 2004; Malhotra & Rhoads 2004; Taniguchi et al. 2005) to detect their Ly α emission lines. Complementary to these photometric surveys, there are some direct spectroscopic approaches based on slitless spectroscopic searches (Kurk et al. 2004; Malhotra et al. 2005) and blind slit searches (Tran et al.

2004; Martin et al. 2006). The Subaru Telescope plays a substantial role in these challenging searches for high- z populations, especially in the Subaru Deep Field (SDF). Our major scientific goal of this project is to construct large samples of LBGs at $z \simeq 4 - 5$ and of LAEs at $z \simeq 4.8, 5.7$ and 6.6 , and make detailed studies of these very high- z galaxy populations. The SDF's wide field imaging increases the chance of discovering rare objects like the most distant galaxies. In addition to the improved detectability, the wide field of view is less subjected to possible large cosmic scatter on the reionization history (Barkana & Loeb 2004; Somerville et al. 2004). Following our first discovery of a couple of LAEs at $z = 6.5$ (z6p5LAEs, Kodaira et al. 2003), Taniguchi et al. (2005, T05) has revealed for the first time a statistically useful sample of nine spectroscopically identified z6p5LAEs, and estimated their total amount of star formation rate density at this high- z end. Nagao et al. (2004, 2005) also serendipitously discovered strong Ly α emissions at $z > 6$ from an i' -drop selected sample in the SDF. Our SDF LAE sample was detected in a general blank field without resorting to amplification of gravitational lensing by foreground clusters, providing reliable statistics about their number density, LF, and cosmic star formation rate density. The high- z survey using gravitational lensing is complementary to our survey, since it detects low-luminosity sources (Ellis et al. 2001; Hu et al. 2002; Santos 2004; Kneib et al. 2004).

In this paper, we report the discovery of eight additional spectroscopically identified z6p5LAEs, which enables a more accurate estimation of their LF. The LF beyond $z = 6$ puts a critical constraint on the reionization epoch as well as on the ionizing photon budget. The Ly α photons are absorbed when passing through neutral IGM, therefore, it is naturally expected that the LF of LAEs should decline as dating back in the reionization epoch. Consequently, the observed abundance of LAEs during the reionization would indicate the neutral fraction of IGM hydrogen $x_{\text{HI}}^{\text{IGM}}$ (Miralda-Escude & Rees 1998). Malhotra & Rhoads (2004) and Stern et al. (2005) found no significant evolution of LFs between $z = 5.7$ and $z = 6.5$, implying that the neutral fraction of the universe is already low at $z = 6.5$. However their LF estimate at $z = 6.5$ was poorly determined, combined from several independent data sets having different selection criteria. On the other hand, there are updated model predictions on the LAE's LF during the reionization epoch (Haiman & Spaans 1999; Le Delliou et al. 2005; Haiman & Cen 2005).

In addition, we evaluate the inhomogeneity of the sky distribution for our z6p5LAE sample. The high- z galaxy survey in a general field also has an advantage in determining their spatial clustering. The i -drop method generally samples a wide redshift range at $5.7 < z < 6.2$, which corresponds to a comoving distance as deep as ~ 200 Mpc along the line of sight. The large-scale structure in this large volume probed by the i -drop method would be diluted in the sky projection, and thus cannot be revealed unless large spectroscopic samples are obtained. On the other hand, NB searches exploring only a small redshift range are more sensitive to the large scale structure, although its thin slice of the universe is, at the same time, likely

to be affected by a cosmic variance (Shimasaku et al. 2004). Inhomogeneous distribution of galaxies beyond $z = 6$ is of high interest not only because of knowing the primeval large scale structure (Stiavelli et al. 2005; Malhotra et al. 2005; Ouchi et al. 2005) but also because it indicates any evidence of patchy reionization, in which Lyman α fluxes are attenuated in one field and not in the other. In the reionization epoch, ionizing sources like LAEs would make cosmological H II regions around them (Miralda-Escude, Haehnelt & Rees 2000). The ionized spheres around adjacent LAEs will overlap, and the space overdensity of these ionizing sources would form a large enough H II region around them to allow high transmission of their Lyman α photons prior to reionization (Wyithe & Loeb 2005; Furlanetto & Oh 2005). The maximum extent of the overlapped ionized region is predicted to be ~ 10 physical Mpc (Wyithe & Loeb 2004; Furlanetto, McQuinn, & Hernquist 2006), which is comparable to the field of view of the SDF. The measurement of inhomogeneity in the spatial distribution of such a high- z population would draw a much more precise picture of the reionization process.

This paper is organized as follows. In § 2, we describe our new spectroscopically identified z6p5LAE sample. In § 3, we derive the Ly α LF of our z6p5LAE sample making comparison with LFs at $z = 5.7$. The estimate of inhomogeneity of sky distribution for our z6p5LAE sample is presented in § 4. We present the composite spectrum of our spectroscopically confirmed z6p5LAE sample in § 5. Some discussions on implications to the reionization based on our results are made in § 6, and the summary of the paper are given in § 7.

Throughout the paper, we analyze in the flat Λ CDM model: $\Omega_m = 0.3$, $\Omega_\Lambda = 0.7$ and $H_0 = 70h_{70}\text{km s}^{-1}\text{Mpc}^{-1}$. These parameters are consistent with recent CMB constraints (Spergel et al. 2006). Magnitudes are given in the AB system.

2. NEW SPECTROSCOPIC CONFIRMATION

Our z6p5LAE photometric candidate sample in the SDF was presented in T05, in which sample selection, star formation rate density of the sample were discussed. The sample was based on the flux excess objects in narrowband $NB921$ ($\lambda_c = 9196\text{\AA}$, FWHM=132 \AA) image compared with the very deep broadband images of the SDF (Kashikawa et al. 2004). Our comoving survey volume was as large as $2.17 \times 10^5 h_{70}^{-3} \text{ Mpc}^3$. In T05, we found 58 photometric candidates of z6p5LAE down to $NB921 = 26.0$ (5σ) in the effective survey region of 876 arcmin 2 , and nine of them had been confirmed as real by spectroscopy. In this section, we describe our extended spectroscopic confirmations of z6p5LAEs after T05. Table 1 summarizes our spectroscopic identifications of $NB921$ -excess objects on the SDF over the last three years. In summary, we have hitherto taken spectroscopy for 22 objects that meet the photometric selection criteria of z6p5LAE, and confirmed that 16 are really LAEs based on their asymmetric line profile, one [O III] emitter, and five faint single line emitters. We have another spectroscopic identified z6p5LAE discovered serendipitously.

2.1. KeckII/DEIMOS spectroscopy

TABLE 1
SUMMARY OF SPECTROSCOPIC IDENTIFICATIONS

Observational run		N_{tot}^a	N_{cand}^b	$\text{Ly}\alpha$	$\text{H}\alpha$	[O III]	[O II]	single line ^c	Ref ^d
2002-2003	Subaru/FOCAS	20	13	10(9) ^e	0	4 ^f	0	3(5) ^e +3 ^f	1,2
2004	KeckII/DEIMOS	14	6	5	1	4	4	0	3
2004	Subaru/FOCAS	19	3	2	1	14	0	2	3

^aThe total object number in which we obtained a spectroscopic signal.

^bThe total object number of z6p5LAE candidates that meet our photometric selection criteria.

^cThese are neither line asymmetry with large S_w as a LAE nor doublet feature as an [O II] emitter.

^dReferences: (1) Kodaira et al. 2002; (2) Taniguchi et al. 2005; (3) This paper.

^eThough 9 LAEs and 5 single line objects were reported in T05, one of the single line objects, SDF J132520.4+273459 was re-observed on 2004 KeckII/DEIMOS run and was found to be a LAE. Another single line object, SDF J132518.4+272122 was concluded to be LAE in this study based on the S_w classification.

^fThe spectra of 4 [O III] emitters and 3 single line objects are obtained as $NB921$ strong emitter on 2002 run.

The z6p5LAE candidates were observed with the KeckII/DEIMOS (Faber et al. 2003) spectrograph on UT 2004 April 23 – 24. We also allocated slits for $NB921$ strong ($z' - NB921 > 1$) emitters irrespective of their ($i' - z'$) color as a LAE criterion in order to see how our selection criteria work. We used four multi-object spectroscopic (MOS) masks with 830 line mm^{-1} grating and an GG495 order-cut filter for each 7000-9000 sec. integration time. The central wavelength was set to 7500Å for one of four MOS masks and 8100Å for other three masks. The slit width was 1.0 arcsec with 0.47Å pix^{-1} giving a resolving power of ~ 3600 . The wavelength coverage was $\sim 5000 - 10000\text{\AA}$, depending on position in the mask. The typical seeing size was 0.55 – 1.0 arcsec during the observation. Our z6p5LAE are almost spatially unresolved on a $NB921$ image with 0.98 seeing size. Assuming that our LAEs were also spatially unresolved on slits, the effective spectral resolution could be better depending on the source size (Rhoads et al. 2003). We also obtained spectra of standard stars BD+28d4211 and Feige110 for flux calibration. The data was reduced with spec2d pipeline¹⁶ for DEEP2 DEIMOS data reduction.

We allocated slits for 18 targets of our z6p5LAE candidates as well as $NB921$ strong emitters. Four of them were apparent [O III] emitters showing their characteristic double lines and sometimes $\text{H}\beta$ also, one is an $\text{H}\alpha$ emitter that has corresponding [O III] emissions, four were [O II] doublets, five have apparently asymmetric single lines, and we did not obtain any signals in four targets.

2.2. Subaru/FOCAS spectroscopy

Three z6p5LAE candidates were also observed with the Subaru/FOCAS (Kashikawa et al. 2002) spectrograph in the MOS mode on UT 2004 April 24 – 27. Although our primary target for this observation was $z = 5.7$ LAE (Shimasaku et al. 2006) in the SDF, three slits were allocated for the z6p5LAE sample. We also allocated slits for strong $NB921$ emitters. The spectroscopy was made with 300 lines mm^{-1} grating and an O58 order-cut filter. The spectra cover 5400 – 10000Å with a pixel resolution of 1.34Å. The 0.6 wide slit gave a spectroscopic resolution of 7.1Å at 9200Å ($R \sim 1300$). The spatial resolution was 0.3/pixel with 3-pixel on-chip binning. The integra-

tion time was 12000-16800 sec. The sky condition was fairly good with seeing of 0.4-0.8 arcsec. The data were reduced in a standard manner. We also obtained spectra of standard stars Hz44 and Feige 34 for flux calibration.

We allocated slits for 21 targets, 14 of them were apparent [O III] emitters showing their double features and sometimes $\text{H}\beta$, one is an $\text{H}\alpha$ emitter that has corresponding [O III] emissions, two have apparently asymmetric single lines, two have symmetric line, and we did not obtain any signals in two remaining targets.

2.3. Spectroscopic result

We combined our spectroscopic sample with those reported in T05, in which nine LAEs and five single emitters are contained. One object SDF J132520.4+273459 which was classified as a single emitter in T05 was re-observed with DEIMOS and was found to be a LAE as shown later with its better quality spectrum. We have also obtained spectra for four [O III] emitters and three single emitters as targets of $NB921$ strong emitters in the same MOS observation, although these objects do not satisfy the LAE criteria and were not reported in T05. The total spectroscopic sample is 53 in this study.

It is difficult to identify a LAE at very high- z with little continuum flux and a tiny signature of $\text{Ly}\alpha$ emission. The asymmetric line profile is the diagnostic of a high- z $\text{Ly}\alpha$ emission, resulting from absorption by neutral hydrogen, therefore it strongly depends upon the ionization structure in and around the high- z objects. Although some bright LAEs show the continuum breaks (Kodaira et al. 2003) caused by the IGM attenuation, most are too faint to detect the break at the highest- z epoch. We have no other spectral features but asymmetric emission profiles that can distinguish high- z LAEs from foreground [O II], [O III], or $\text{H}\alpha$ emitters. To quantify this asymmetry accurately, we introduced an asymmetry statistics *skewness* S and *weighted skewness* S_w . Here we regarded the observed spectrum, which is basically a 2-dimensional array of the flux (f_i) and the pixel (x_i), as a distribution function with an array size of n . The S is defined as,

$$S = \frac{1}{I\sigma^3} \sum_i^n (x_i - \bar{x})^3 f_i, \quad (1)$$

where $I = \sum_i^n f_i$, and \bar{x} , σ are the average and dispersion of x_i , respectively. The S indicator has an ad-

¹⁶ The data reduction pipeline was developed at UC Berkeley with support from NSF grant AST-0071048.

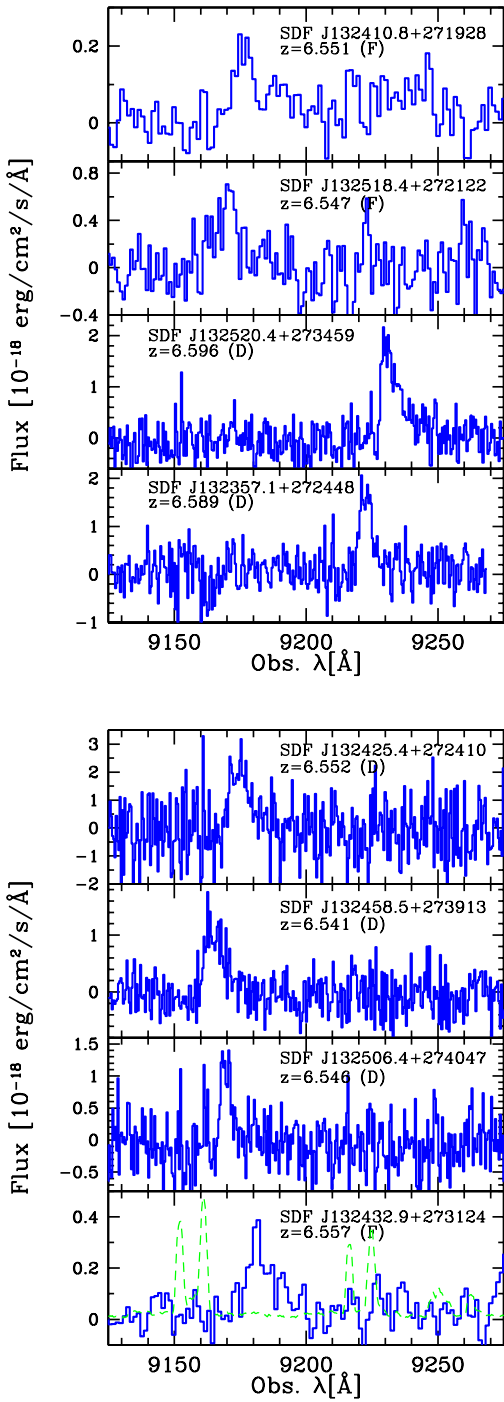


FIG. 1.— Spectrum of eight spectroscopically confirmed 6p5LAEs. “F” (“D”) in parentheses indicates that the object was observed with FOCAS (DEIMOS). The sky spectrum is overplotted on the bottom panel with arbitrary flux scale. The spectrum of SDF J132518.4+272122 which was identified as a LAE in this study already appeared in T05.

vantage of being independent of line profile modeling or fitting procedure. Our statistics S has a good correlation with other asymmetry indicators a_λ or a_f (Rhoads et al. 2003) as shown in the appendix.

The *weighted skewness* S_w is the revised indicator of S

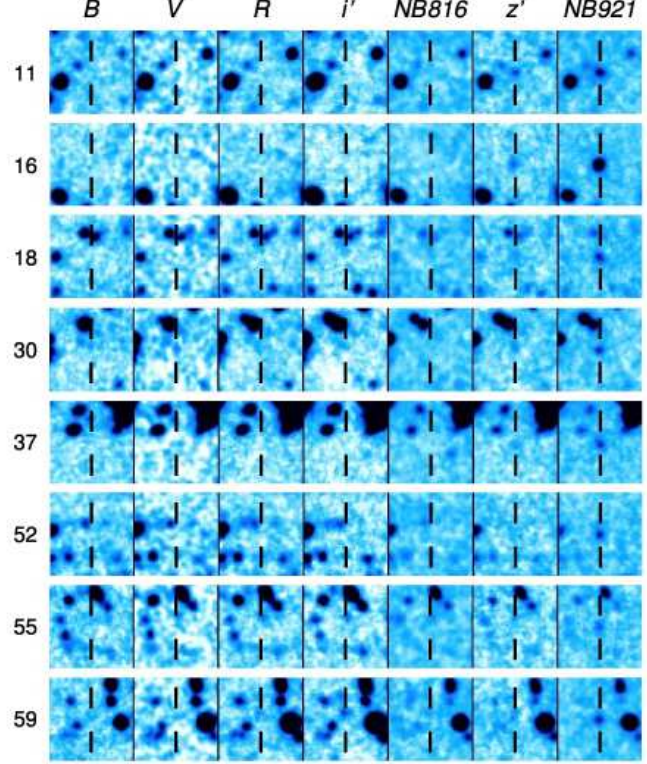


FIG. 2.— Thumbnail images of our eight identified LAEs. The object IDs are those of T05, except ID=59 which is not listed in the photometric catalog of T05. B , V , R , i' , $NB816$, z' , and $NB921$ -band images are shown from left to right. Each image is $10''$ on a side. North is up and east is left.

so as to be more sensitive to an asymmetry, although it depends on the fitting procedure. We define the *weighted skewness* S_w as,

$$S_w = S(\lambda_{10,r} - \lambda_{10,b}), \quad (2)$$

where $\lambda_{10,r}$ and $\lambda_{10,b}$ are the wavelength where the flux drops to 10% of its peak value on the red and blue sides of the Ly α emission, respectively.

In this study, we classified our observed emission lines based on the S_w indicator as shown in the appendix. Table 1 summarizes the identifications for our 53 spectra. We have identified apparent foreground emitters, two H α emitters, 22 [O III] emitters, four [O II] emitters, by their multiple emission line signatures. The properties of these emission line galaxies at $z < 1.2$ will be presented in our forthcoming paper (Ly et al. 2006). The S_w value of these apparent foreground emitters never exceeds $S_w = 3$, which we set as the critical S_w value to distinguish LAEs from foreground emitters. This critical value is the same as for our $z = 5.7$ LAE sample (Shimasaku et al. 2006). As a result, we have so far obtained 17 LAEs at $z = 6.5$. All of the nine LAEs identified in T05 were classified as LAEs with S_w , and we obtained eight additional spectroscopic confirmations

TABLE 2
SPECTROSCOPIC PROPERTIES OF $z = 6.5$ LAEs

ID ^a	Name	z^b	$f^{\text{spec}}(\text{Ly}\alpha)^c$ (10^{-18} ergs/s/cm 2)	$L^{\text{spec}}(\text{Ly}\alpha)^d$ ($10^{42} h_{70}^{-2}$ ergs/s)	$\text{SFR}^{\text{spec}}(\text{Ly}\alpha)^{d,e}$ (M_{\odot}/yr)	FWHM ^f (Å)	S_w (km/s)	Obs. ^g
11	SDF J132410.8+271928	6.551	5.39	2.64	2.40	14.6	477	7.05 ± 4.79
16	SDF J132518.4+272122	6.547	11.2	5.47	4.98	11.0	360	4.75 ± 2.35
18	SDF J132520.4+273459	6.596	10.0	4.97	4.52	8.2	266	11.58 ± 0.54
30	SDF J132357.1+272448	6.589	10.6	5.25	4.78	5.9	192	3.12 ± 0.30
37	SDF J132425.4+272410	6.552	14.5	7.09	6.45	8.9	291	16.34 ± 0.44
52	SDF J132458.5+273913	6.541	7.67	3.74	3.40	9.7	318	7.63 ± 0.71
55	SDF J132506.4+274047	6.546	9.84	4.80	4.36	6.3	206	3.77 ± 0.44
59	SDF J132432.9+273124	6.557	4.50	2.20	2.00	11.0	359	4.22 ± 2.50

^aThe object IDs are those of T05, except ID=59 which is not listed in the photometric catalog of T05.

^bThe redshift was derived from the wavelength of the flux peak in an observed spectrum assuming the rest wavelength of Ly α to be 1215Å. These measurements could be overestimated in the case of significant damping wings by IGM, also the observed peak position was slightly shifted redward due to instrumental resolution. See Figure 9.

^cThe observed line flux just measured the total amount of the flux within the line profile.

^dNo dust absorption correction is applied.

^eEstimated from the observed luminosities with the relation $SFR(\text{Ly}\alpha) = 9.1 \times 10^{-43} L(\text{Ly}\alpha) M_{\odot} \text{ yr}^{-1}$ as in T05.

^fCorrected for instrumental broadening.

^gObserved with FOCAS(F) or DEIMOS(D).

of LAEs in this study¹⁷. The spectra of newly identified LAEs in this study are shown in Figure 1, and their spectroscopic properties are summarized in Table 2. For all of the eight LAE spectra, we did not detect any UV continuum fluxes significant enough to measure their equivalent widths reliably. Nor did we detect N V λ 1240, the only accessible strong high-ionization metal line indicative of AGN activity. We will discuss their composite spectrum in § 5. Figure 2 presents postage stamp images in all the seven bands of these eight LAEs.

We have also eight single line emitters in which we detected neither asymmetric line having large S_w as a LAE, nor doublet features as in [O II] emitter. Probably most of them are unresolved [O II] doublet lines, based on their small S_w . In fact, all of these single lines were observed by Subaru/FOCAS, whose data lacked the resolving power to separate the [O II] doublet ($\Delta\lambda = 6.64$ Å) at 9160Å. Our 58 photometric LAE candidates down to $NB921 = 26.0$ (5σ) were selected in T05 based on criteria $z' - NB921 > 1$, $z' - NB921 > 3\sigma$ and $i' - z' > 1.3$ at $i' \leq 27.87$ (2σ) and simply $z' - NB921 > 1$ at $i' > 27.87$ (2σ). Also we adopted another criterion for LAE candidates of no detections ($< 3\sigma$) in deep B , V , and R -band images. The 53 objects for which we obtained spectra are composed of LAE candidates and $NB921$ -strong emitters. Among these 53, 22 objects meet the criteria for our photometric sample, 16 are LAEs, one [O III] emitter, and five single line emitters. We have another spectroscopically identified LAE which was not listed in the LAE candidate list by T05. The object is listed as No.59 in Table 2, and is found to have a very close neighbor in i' -band image (see Figure 2), which failed a correct aperture photometry. 16 LAEs that meet our selection criteria out of our spectroscopic LAE sample of 17 indicate $16/17 = 94\%$ sample completeness, provided that all of eight single emitters are foreground. Otherwise, the sample completeness is $(16 + 5)/(17 + 8) = 84\%$ at

¹⁷ SDF J132518.4+272122 has been classified as a single emitter in T05, although it shows a very red color ($i' - z' > 2.21$) and high enough S (0.173) and S_w (4.75) values. Therefore it was classified as a LAE in this study.

most if all of single emitters are z6p5LAEs. The simple average of these two extreme cases, 89%, is regarded as the sample completeness. On the other hand, the sample contamination rate is estimated as follows. One [O III] emitter satisfies our LAE criteria¹⁸ and five single emitters satisfied our LAE criteria, suggesting a $1/22 = 4.5\%$ contamination rate. The contamination rate could be $(1 + 5)/22 = 27\%$ at most if all of these five single emitters were foreground objects. The contamination rate is estimated to be 16% taking the average of these two cases. Therefore our sample reliability factor, determined as the ratio of the number of true LAEs to the number of objects that meet our selection criteria, is evaluated to be $(1 - 0.16)/0.89 = 0.94$. One object found to be an apparent [O III] emitter by spectroscopy was removed from the photometric sample, while one LAE, which happened to be found by spectroscopy but not listed in the original candidate sample of T05 was included in the photometric sample. In the further analysis below, we used this photometric sample. We have six objects, in which we did not obtain any signals in spectroscopy. Five of them have $NB921 > 25.5$, which is almost close to current spectroscopic limit.

Figure 3 shows the peak wavelength distribution of 17 confirmed LAEs as well as 28 foreground emitters within the $NB921$ bandpass. The distribution of LAEs apparently shows a systematic deviation to the blue side of the NB transmission curve in contrast to the symmetric distribution of foreground emitters. This is due to the fact that the LAE profile, having a broad red wing and sharp blue cutoff as well as Lyman continuum break, makes a larger NB excess when it lies at the shorter side of the transmission curve. This was also the case for LAE survey at $z = 5.7$ with $NB816$ (Shimasaku et al. 2006; Hu et al. 2004).

3. LY α LUMINOSITY FUNCTION

We estimated the LF of z6p5LAE based on both our spectroscopic z6p5LAE sample of 17 and our photo-

¹⁸ No.29 in T05. This object is located near a bright star from which the accurate photometry is prevented.

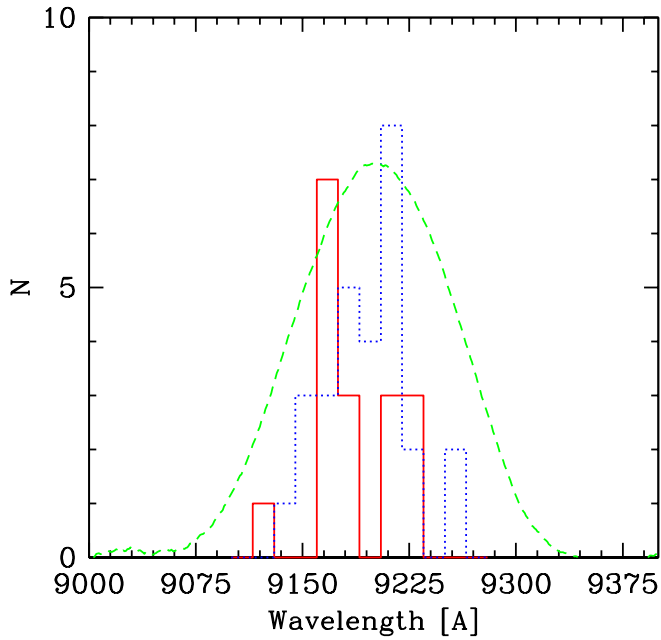


FIG. 3.— The observed wavelength distribution of the Ly α line peak for our 17 z6p5LAE sample (red solid histogram), and our foreground sample (blue dotted histogram). The transmission profile of NB921 is overplotted (green dashed line).

metric z6p5LAE sample of 58. The LF can be simply derived from the number density of confirmed LAEs multiplied by the spectroscopic confirmation fraction (Malhotra & Rhoads 2004, T05); however, the uncertainties of the fraction inevitably depend on the magnitude because spectroscopic confirmation is more difficult at fainter magnitudes. Thus we estimated the range of acceptable z6p5LAE LFs as specified by the upper and lower limits.

The lower limit to the z6p5LAE LF is based on our spectroscopic z6p5LAE sample of 17, whose Ly α emissions have been surely detected, although this sample is incomplete. While the upper limit was estimated from the combined spectroscopic and photometric samples. The fluxes of Ly α emission and rest UV continuum (at 9500Å) of our photometric sample were inferred from the photometry of NB921 and z' -band using the equations, (7) and (6) of T05, respectively. Note that we derive the apparent Ly α luminosity uncorrected for either the dust extinction or the self-absorption evident on the blue side cutoff of the emission line. The comparison of Ly α fluxes

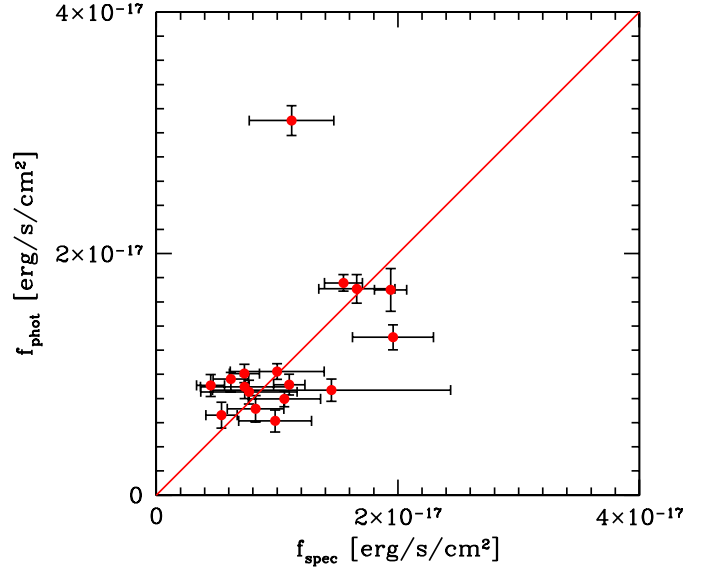


FIG. 4.— The comparison of the Ly α fluxes measured by spectra, f_{spec} with those inferred from photometry, f_{phot} for our spectroscopic z6p5LAE sample. The solid line represents a one-to-one correspondence between f_{spec} and f_{phot} . The errors were estimated based on the sky rms fluctuation on each spectra for f_{spec} , and errors on magnitudes for f_{phot} . One object far out of agreement is found to have a spectrum affected by bad columns.

measured spectroscopically with those inferred from photometry for our spectroscopic z6p5LAE sample is shown in Figure 4. The correspondence is good except in a few cases. One object far out of agreement is found to have a spectrum affected by bad columns. We therefore used the photometric inferred Ly α fluxes for the remaining 41 ($= 58 - 17$) photometric sample.

We have to correct for a detection completeness, which could crucially affect the result when calculating the LF based on a deep photometric catalog. The detection completeness as a function of apparent NB921 magnitude was estimated in almost the same way as in Kashikawa et al. (2004), that is, by counting detected artificial objects distributed on the real NB921 image. We assume Gaussian profiles for these artificial objects with FWHM = 1.¹³, which is the nominal size of our z6p5LAEs sample (T05). The detection completeness was thus evaluated as $> 75\%$ for $NB921 < 25.0$ and 45% at the limiting magnitude $NB921 = 26.0$. In the upper limit estimate, we corrected for this detection completeness of each sample by number weighting according to the NB921 magnitude. Note that the upper limit can be regarded as our current best estimate for z6p5LAE LF, because it is properly corrected for the detection incompleteness.

Figure 5 shows the cumulative Ly α LF of our z6p5LAE sample. The open red circles denote the raw counts of spectroscopic + additional photometric sample, and the solid red circles are those with corrected detection com-

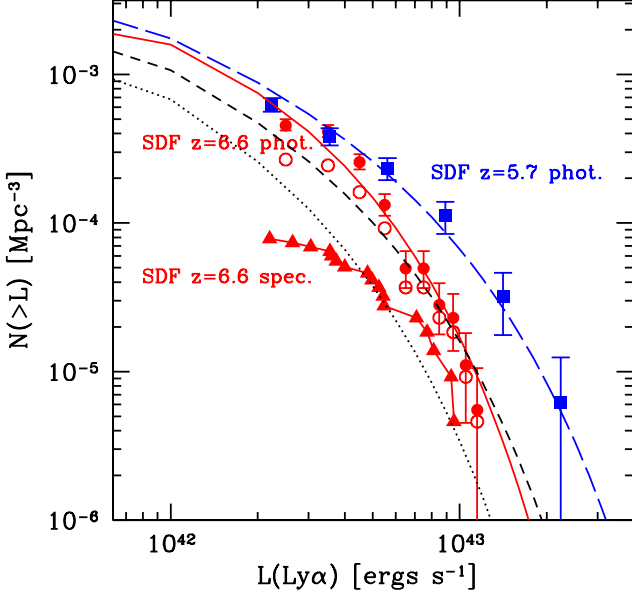


FIG. 5.— The cumulative Ly α LF of our z6p5LAE sample. The open red circles denote the raw counts of our spectroscopic sample + additional photometric sample, and the solid red circles are those with corrected for detection completeness (upper limit). The red solid triangles denote the raw counts of the pure spectroscopic sample (lower limit). Error bars for the solid circles are Poissonian. The blue squares and long-dashed line show the LF of LAEs at $z = 5.7$ evaluated on the SDF (Shimasaku et al. 2006). The short-dashed and dotted lines show the Schechter luminosity functions, in which the Ly α luminosities are reduced by a factor of 0.6 ($L^* \times 0.6$) and 0.4 from the $z = 5.7$ LF, respectively.

pleteness. The red solid triangles denote the raw counts of the pure spectroscopic sample. Therefore, the solid triangle and circles are the lower, and upper limits, respectively, of our estimates of z6p5LAE LF. The error bars on the solid circles just denote the Poisson errors, although there could be other plausible but immeasurable error sources such as an ambiguity in inferring the Ly α luminosity from photometric data. Taking into account the corrections with respect to the sample reliability factor (94%) evaluated in the previous section, the LF has a margin to go upwards by a factor of 1.06, although this uncertainty is smaller than the Poisson errors. We fit a Schechter function, $\phi(L)dL = \phi^*(L/L^*)^\alpha \exp(-L/L^*)dL/L$, to our z6p5LAE LF. The χ^2 was minimized with a single grid search in the two parameters, L^* and ϕ^* for fixed slope of $\alpha = -2.0, -1.5$, and -1.0 . The derived best-fit parameters are listed in Table 3.

The blue squares and dashed line in Figure 5 show the LF of LAEs at $z = 5.7$ evaluated in the SDF (Shimasaku et al. 2006). This is the most reliable estimate so far because of its deeper photometric sample and more spectroscopically confirmations than that of Hu et al. (2004). In addition, it is worth noting that this LAE sample at $z = 5.7$ was selected from the same field

TABLE 3
BEST-FIT SCHECHTER PARAMETERS FOR LAE LF AT $z = 6.5$ AND 5.7 OF THE SDF

sample	α (fix)	L^* $\log(h_{70}^{-2} \text{ ergs s}^{-1})$	ϕ^* $\log(h_{70}^3 \text{ Mpc}^{-3})$
z=6.5	upper limit	-2.0 $42.74^{+0.14}_{-0.14}$	$-3.14^{+0.30}_{-0.34}$
	-1.5	$42.60^{+0.12}_{-0.10}$	$-2.88^{+0.24}_{-0.26}$
	-1.0	$42.48^{+0.10}_{-0.08}$	$-2.74^{+0.18}_{-0.22}$
	lower limit	-2.0 $43.30^{+0.23}_{-0.61}$	$-4.80^{+1.02}_{-0.20}$
	-1.5	$42.95^{+0.78}_{-0.42}$	$-4.17^{+0.70}_{-0.83}$
	-1.0	$42.75^{+0.48}_{-0.32}$	$-3.88^{+0.51}_{-0.57}$
z=5.7	-2.0	$43.30^{+0.22}_{-0.18}$	$-3.96^{+0.28}_{-0.30}$
	-1.5	$43.04^{+0.12}_{-0.14}$	$-3.44^{+0.20}_{-0.16}$
	-1.0	$42.84^{+0.10}_{-0.10}$	$-3.14^{+0.14}_{-0.12}$

and the same photometry as this study, having similar survey volume and similar selection criteria. For example, we have carefully determined the NB -excess criteria so as to have almost the same equivalent width ($EW > 20\text{\AA}$ in rest-frame) thresholds for both of these LAE samples. According to previous studies, the LF of LAEs between $z = 3$ and $z = 6$ is almost unchanged (Tran et al. 2004; van Breukelen, Jarvis & Venemans 2005). The LAE population appears quite similar number density in all the epoch. The comparison of the LAE LF with previous studies at $z \leq 5.7$ is shown in a companion paper by Shimasaku et al. (2006), which confirmed that the LF of LAE at $z = 5.7$ is almost identical to those in lower- z . However, our z6p5LAE LF shows an apparent deficit at the bright end in both upper and lower limit estimates. The L^* difference between $z = 6.5$ (the upper limit) and $z = 5.7$ is a factor of ~ 2 corresponding ~ 0.75 mag assuming a fixed $\alpha = -1.5$. We have already spectroscopically identified almost all (4 confirmed out of 6 candidates at $NB921 \leq 25.0$) of our bright LAE candidates, so this resultant deficit at the bright end would not significantly change even if we obtain more follow-up spectroscopy in future. Moreover, uncertainties on the detection completeness correction and the selection effects according to the equivalent width of the Ly α line are expected to be small at the bright end. As seen in Figure 4, there are possible but unsystematic errors in inferring the Ly α luminosity from photometric data, which could affect the resultant LF in some degree. When using only the photometric inferred Ly α luminosities for all of our 58 sample, the best-fit Schechter parameters only change $\Delta \log(L^*) = 0.04$ and $\Delta \log(\phi^*) = 0.1$ at most for $-2.0 < \alpha < -1.0$, which are negligible. Moreover, we carried out a Monte Carlo simulation to see a possible distortion that the discrepancy between spectroscopic measured and photometrically inferred Ly α luminosities could cause on the resulted LF. We re-calculated the LF in many times after assigning a random error perturbed within the same scatter as in Figure 4 to each Ly α luminosity. With this simulation, the best-fit Schechter parameters vary with rms fluctuations of $\sigma(\log(L^*)) = 0.019$ and $\sigma(\log(\phi^*)) = 0.032$ for fixed $\alpha = -1.5$, suggesting again that the possible errors in inferring the Ly α luminosity are expected to be small.

At lower- z ($z = 3.0 - 5.7$), several LAEs with large

$L(\text{Ly}\alpha) > 2 \times 10^{43} h_{70}^{-2}$ erg s $^{-1}$ have been actually identified by spectroscopy with much higher number density (Shimasaku et al. 2006; Hu et al. 2004; Maier et al. 2003; Kudritzki et al. 2000; Cowie & Hu 1998), while our z6p5LAE sample has no spectroscopically confirmed object having such a large Ly α luminosity. There are three other LAEs at $z \sim 6.5$ that have been spectroscopically identified so far in independent surveys (Rhoads et al. 2004; Kurk et al. 2004; Stern et al. 2005) without taking advantage of the amplification by a foreground gravitational lens. All of these LAEs also have similar Ly α luminosity as $L(\text{Ly}\alpha) = 1.04 - 1.1 \times 10^{43} h_{70}^{-2}$ erg s $^{-1}$ that is consistent with our brightest LAEs.

On the other hand, at fainter luminosities of $L(\text{Ly}\alpha) < 5 \times 10^{42} h_{70}^{-2}$ erg s $^{-1}$, our upper limit estimate of z6p5LAE LF almost reaches to the same amplitudes as at $z = 5.7$, although the amplitude difference between our upper and lower limits is too large to determine its faint end. Our faint spectroscopic sample is still so small that we cannot conclude yet whether there is a significant difference between $z = 6.5$ and $z = 5.7$ at the faint end of the LF. In this study, we cannot determine the faint end slope of the LAE LF at $z = 6.5$, and consequently it is difficult to constraint on the true contribution of LAE population to the entire photon budget required for the fully reionization.

Malhotra & Rhoads (2004) and Stern et al. (2005) found no significant evolution of LAE LF from $z = 6.5$ to $z = 5.7$. However, their estimates were based on small samples combined from various independent data set with different selection criteria. Our z6p5LAE sample is selected with the same criteria from the large homogeneous sample in a general field without resorting amplification of gravitational lens. The uncertainty of detection completeness estimate could not be large, at least at the bright end. Moreover, our survey comoving volume is comparably large as those others at $z = 5.7$ (Shimasaku et al. 2006; Hu et al. 2004). As seen in Figure 3, our effective survey depth is smaller than that estimated from the FWHM of the narrow-band filter; however it is more or less the similar case for $z = 5.7$ LAE sample and its correction would not affect the result (Shimasaku et al. 2006). Therefore our LF estimate of z6p5LAE is highly reliable, although we cannot completely rule out the possibility that the deficiency at the bright end is caused by a cosmic variance.

To see the significance of the LF difference between $z = 6.5$ and $z = 5.7$, we plot the error contours in Figure 6 for our Schechter-parameter fits. In this case, we compare only the upper limit LF estimate which is the current best estimate for our z6p5LAE sample and is more crucial to conclude whether the LF difference with $z = 5.7$ is significant or not. The confidence levels of the fitting were computed based on Poissonian error statistics. The best-fit parameters of $z = 5.7$ LF is slightly different from those presented in Shimasaku et al. (2006), in which Schechter parameters were determined so as to be consistent with the NB816 number count. In contrast, here we determined these parameters simply by fitting Schechter function to the data points. Figure 6 reveals that the (L^*, ϕ^*) parameter error ellipses of $z = 5.7$ and $z = 6.5$ do not overlap each other for any α , that is, the difference of LF between $z = 5.7$ and $z = 6.5$ is significant at more than the 3σ level.

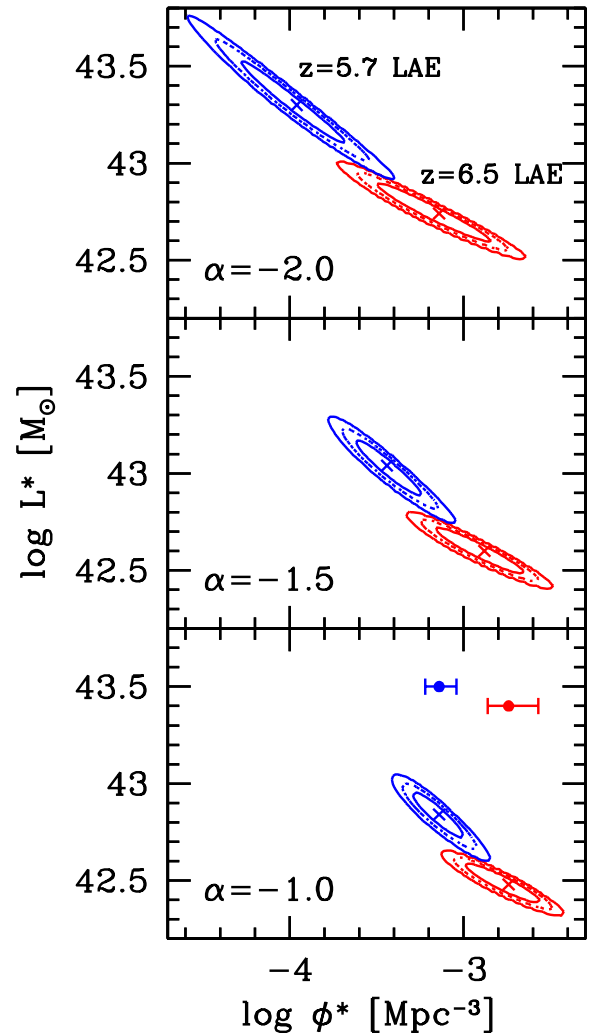


FIG. 6.— The error ellipses of the best-fit Schechter parameters ϕ^* and L^* for each fixed α value. The red ellipses are for the z6p5LAE upper limit sample, while the blue ellipses are for the z5p7LAE sample of Shimasaku et al. (2006). The inner and outer solid ellipses are the 1σ and 3σ confidence levels, respectively. The dotted ellipses show the 2σ confidence levels. The error bars in the lower panel correspond to the uncertainty in ϕ^* due to the cosmic variance (Somerville et al. 2004).

The parameter L^* difference is more significant than the ϕ^* difference. Based on Somerville et al. (2004), we evaluated the cosmic variance of our z6p5LAE sample. We assumed a one-to-one correspondence between LAEs and dark haloes, and used their predictions at $z = 6$. With the comoving survey volume of $2.17 \times 10^5 h_{70}^{-3}$ Mpc 3 and the number density of $2.67 \times 10^{-4} h_{70}^3$ Mpc $^{-3}$ (7.83×10^{-5}) for upper (lower) limit estimate, we obtain the cosmic variance as $\sim 32\%$ ($\sim 37\%$). Also we estimated $\sim 20\%$ variance for the $z = 5.7$ LAE sample. The possible field-to-field variance on the LF at $z = 5.7$ can be seen on the Figure 11 of Shimasaku et al. (2006). As shown by the error bars in Figure 6, the error circles overlap each other within 3σ significance when taking into account the cosmic variance; however, our upper limit estimate still is different from that of $z = 5.7$ at 2σ significance.

4. REST UV CONTINUUM LUMINOSITY FUNCTION

In the previous section, the flux of rest UV continuum (at 9500Å) was simultaneously derived from the photometry of *NB921* and z' bands. We derive the rest UV (1255Å at $z = 6.57$) continuum LF based on our 58 photometric sample. We take into account the correction of detection incompleteness in *NB921* when calculating the LF, though the correction should be actually based on the completeness measured in z' -band which corresponds to the rest UV flux. However, our Ly α selected sample is basically constructed from the *NB921* magnitude limited sample, it is inevitable that the derived rest UV continuum LF could be affected, especially at the faint end of the LF, by the discrepancy of completeness in between *NB921* and z' bands. This is also the case for other LAE studies (Shimasaku et al. 2006; Hu et al. 2004).

Figure 7 shows the rest UV continuum LF of our z6p5LAE sample compared with other studies at similar redshifts. No correction has been applied for dust. The vertical lines indicate the corresponding limiting magnitudes in z' -band. Our LF measurements at fainter than $M_{UV} = -20.24(3\sigma)$ might be uncertain because corresponding z' -band magnitudes are no longer reliable. We overplot in Figure 7 other rest UV continuum LF estimates of the LAE sample at $z = 5.7$ evaluated in the SDF (Shimasaku et al. 2006), the *i*-dropout objects at $z \sim 6$ by Bouwens et al. (2005), and the LAE sample at $z = 5.7$ by Hu et al. (2004). We here neglect a slight difference of corresponding rest-frame wavelengths ($\sim 1350\text{\AA}$ at $z = 5.7$ and $\sim 1255\text{\AA}$ at $z = 6.5$), assuming a flat far-UV spectral energy distribution. Our measurement agrees with these two studies very well at $M_{UV} < -20.5$. The agreement at the bright end of rest UV continuum LF between $z = 6.5$ and 5.7 is in clear contrast with that seen in the Ly α luminosity LF. It should be noted that the rest UV continuum luminosity is not attenuated by neutral IGM and is less affected by dust extinction than the Ly α luminosity. As far as the rest UV continuum LF, the cosmic variance is not severe among these samples. The flatter faint end slope of the LFs of LAE samples at both $z = 6.5$ and 5.7 than that of *i*-dropouts at $z \sim 6$ could be caused by the detection incompleteness of LAE sample.

5. CLUSTERING PROPERTIES

Our 58 z6p5LAE candidates have been extracted from a very wide field of view ($34' \times 27'$). We tried to detect any clustering signal in the z6p5LAE sample by several methods. We derived the angular two-point correlation function (ACF) $w(\theta)$ using the Landy & Szalay (1993) estimator. 100,000 random points were created in exactly the same boundary conditions as the SDF galaxy catalog, avoiding the mask regions in which saturated stars dominate. The upper panel of Figure 8 shows the ACF for z6p5LAE. Solid circles denote the ACF for all the 58 z6p5LAE sample, while open squares denote the 53 z6p5LAE sample removing five single line emitters. We did not correct for the integral constraint which is negligible in the SDF (Kashikawa et al. 2006). We estimated only Poissonian errors of the ACF as, $\sigma_w(\theta) = \sqrt{(1 + w(\theta))/DD(\theta)}$, where the $DD(\theta)$ is the number of random-random pairs having angular separa-

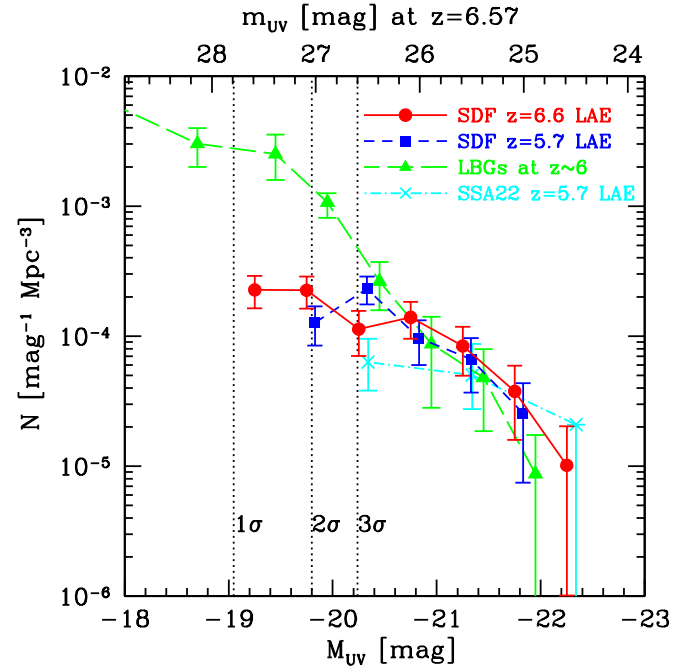


FIG. 7.— The rest-UV (1255Å at $z = 6.57$) continuum LF of our z6p5LAE sample (red circles and solid line). As a comparison, the blue squares (and short dashed line) are the rest UV LF of the LAE sample at $z = 5.7$ evaluated in the SDF (Shimasaku et al. 2006), the green triangles (and long dashed line) are of the *i*-dropout objects at $z \sim 6$ by Bouwens et al. (2005), the cyan crosses (and dot dashed line) are of the LAE sample at $z = 5.7$ by Hu et al. (2004). The vertical lines indicate the limiting magnitudes in z' -band at $M_{UV} = -19.05, -19.80$ and -20.24 for $1\sigma, 2\sigma, 3\sigma$, respectively. Error bars are Poissonian.

tion θ . The result shows that the amplitude is almost zero for all scales, indicating the sample has an almost homogeneous distribution. However, our z6p5LAE sample is so small that the derived ACF has a large ambiguity. Therefore we tried two other methods that are more robust for small-number statistics to quantify the clustering strength.

First, we applied the two-dimensional Kolmogorov-Smirnov test to our sample. The two-dimensional Kolmogorov-Smirnov test is generalized by Peacock (1983) to give the integral probability of distribution in four quadrants around a certain point. To see the difference from homogeneous distribution, we generated random points as was the case with our ACF estimate. We found our z6p5LAE sample was equivalent to a homogeneous distribution at the 83.3% (83.8% after removing five single line emitters) confidence level.

Second, we estimated the void probability function (VPF). The VPF is defined as the probability of having no galaxies in a randomly placed sphere of radius R , or in a circle of angular radius θ in case of a two-dimensional sky distribution. The VPF is known to be related to the hierarchy of n -point correlation functions (White 1979). We adopted the same technique as Croton et al. (2004) to correct for the irregular geometry of the survey region.

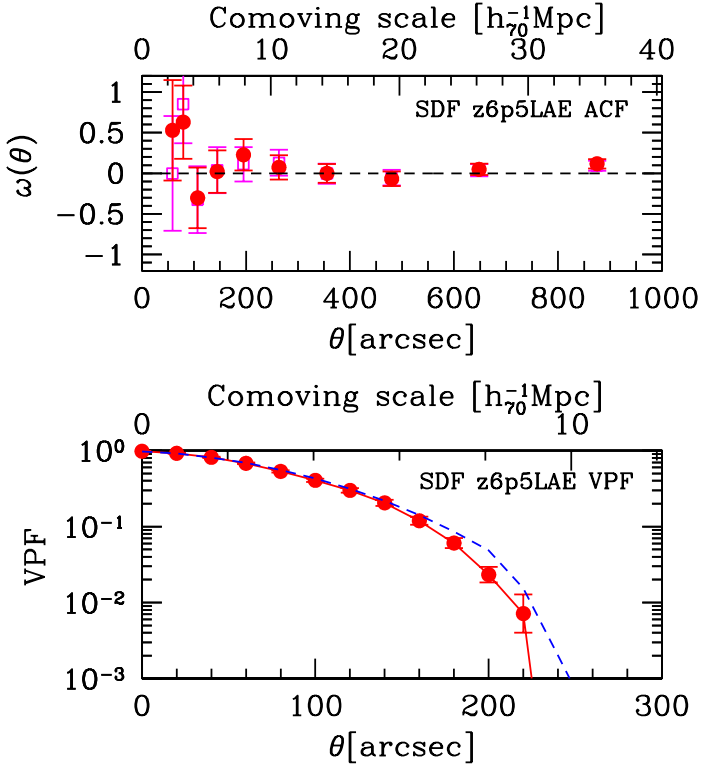


FIG. 8.— The upper panel shows the ACF of our z6p5LAE sample. The solid circle denotes the ACF for all the 58 z6p5LAE sample, while open squares denote that of 53 z6p5LAE sample in which five single line emitters are removed. Error bars show the 1σ Poissonian errors. The lower panel shows the VPF of our z6p5LAE sample (red solid circles). The blue dashed line is the VPF of a random sample.

The result is shown as a solid line in the lower panel of Figure 8, compared with that of a random sample indicated by the dashed line. No excess of VPF was found for our z6p5LAE sample relative to the random sample.

The above three estimates indicate that the spatial distribution of the z6p5LAE sample is homogeneous. The results were identical for all three estimates even if we divided our sample into brighter/fainter subsamples. The homogeneous distribution of z6p5LAEs is in contrast to the lower- z where LAE populations are often found to trace the large-scale structures even in blank fields (Steidel et al. 2000; Shimasaku et al. 2003; Palunas et al. 2004; Ouchi et al. 2005). As in the previous section, we estimated the cosmic variance as $\sim 32\%$ at most. We should note that NB searches exploring only a small redshift coverage are also sensitive to the large scale structure (Shimasaku et al. 2004). We cannot deny the possibility that we happen to see a very homogeneous region of the $z = 6.5$ universe. A survey with much larger volume is required for further discussions.

6. LY α PROFILE OF THE COMPOSITE SPECTRUM

Although each spectrum of our 17 z6p5LAEs has too low S/N to infer either inter-dynamics of LAE itself or IGM characteristics (e.g., Haiman 2002) the composite spectrum could be useful to see the general spectroscopic properties of the z6p5LAE population. We have 17 z6p5LAE spectra at different spectroscopic res-

olution. First, we removed 5 spectra¹⁹ that have been taken with the poorest instrumental resolution. Then, each spectrum was smoothed with adequate Gaussian kernel chosen to produce a common instrumental resolution of FWHM = 6.41 Å. The instrumental resolution for each spectrum was practically measured by the FWHM of sky lines near the Ly α emission. The redshift was measured based on the line peak wavelength, then shifted to the mean redshift $\langle z \rangle = 6.556$ rebinned to a common pixel scale. In the process, we neglected possible systematic offsets of Ly α lines from the rest-frame established by other lines, which is often found in LBG spectra (Shapley et al. 2003). The spectra were then combined by taking the average after scaling according to their peak line flux.

The upper panel of Figure 9 shows the final composite spectrum of our 12 z6p5LAE sample. The composite spectrum reveals apparently asymmetric profile with an extended red wing, which is clearly seen through a comparison with a Gaussian profile (denoted by dotted lines) corresponding to the final instrumental resolution. The skewness and weighted-skewness of the composite spectrum are $S = 0.542 \pm 0.007$, and $S_w = 11.466 \pm 0.156$, respectively. The blue side of the line profile is almost explained only by the instrumental resolution blur, as also concluded in Hu et al. (2004); Westra et al. (2005). Assuming that an intrinsic Ly α profile is a simple Gaussian at almost the same peak position as observed, and completely truncated at the blue side of the line, the resultant profile convolved with the instrumental resolution did not coincide with the observed profile producing a large red wing anomaly. The disagreement is inconsistent with the result for $z = 5.7$ case by Hu et al. (2004).

To explain the observed profile, we considered two plausible models. The first model is the “galactic wind model” which was motivated by the similar analogy of Dawson et al. (2002); Mas-Hesse et al. (2003). If galactic winds are present, the far side of the expanding shell back-scatters redshifting Ly α photons that would make another broadly extended Gaussian component in their line profile. We simply assumed that the Ly α photons from the blue side of the object redshift are completely absorbed by neutral hydrogen at near side in line of sights. This model is composed of two Gaussian profiles; one is a high-amplitude and narrow Gaussian which originates from recombination Ly α photons in the central H II region, and the other is a low-amplitude broad Gaussian from back-scattered Ly α photons by a galactic wind. The middle panel of Figure 9 shows the best-fit galactic wind model. The resultant profile is shown by the red solid line, which is the combination of narrow and broad Gaussians convolved with instrumental resolution. It perfectly explains the observed profile. The best-fit parameters are listed in Table 4. The picture of large-scale outflowing of gas with velocities ~ 200 km s $^{-1}$ is in good agreement with those of nearby H II galaxies (Kunth et al. 1998), while somewhat smaller than those of $z \sim 3$ LBGs (Pettini et al. 2002) and $z \sim 5$ LAEs (Dawson et al. 2002; Westra et al. 2005).

The second model is the “reionization model”, in which the intrinsic Ly α line has a larger amplitude than that observed and its peak wavelength is much shorter than

¹⁹ The removed sample were object ID=4, 5, 6, 7, and 8 in T05

TABLE 4
MODEL PARAMETERS FOR COMPOSITE LY α PROFILE OF LF OF Z6P5LAE

model	component	λ_c (Å)	Amplitude (ergs s^{-1} cm^{-2} \AA^{-1})	σ (Å)	offset (km s^{-1})
galactic wind model	central HII	9183.3	2.11E-17	3.32 108.5	-2.34 -76.5
	galactic wind	9191.6	3.31E-18	7.93 259.2	+5.97 +195.1
reionization model		9179.9	9.00E-17	6.50 212.4	-5.70 -186.3

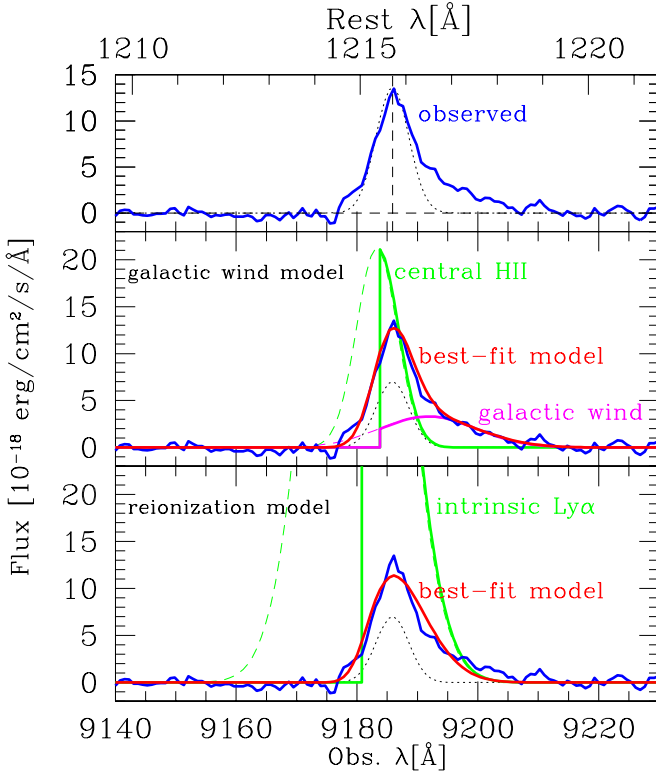


FIG. 9.— The blue spectrum of each panel shows the final composite spectrum of our 12 z6p5LAE sample. The black dotted line denotes a Gaussian profile corresponding to the instrumental resolution. The middle panel shows the best-fit galactic wind model. The resultant profile is shown as the red solid line, which is the combination of narrow (green line) and broad (magenta line) Gaussians convolved with instrumental resolution. The lower panel shows the reionization model. The resultant profile is shown by a red solid line, which is the combination of the intrinsic Ly α profile (green line) and damping wing attenuation convolved with the instrumental resolution. See Table 4 for the best-fit parameters for each model.

the observed peak position. Such a picture is generally predicted for the Ly α profile in the reionization epoch (Haiman 2002; Santos 2004). The Ly α photons would be absorbed by both the red damping wing of the Gunn-Peterson trough from outside the cosmological H II region, and the residual neutral hydrogen inside the H II region. The latter true contribution is not yet known, thus we here simply assumed that the inside of the H II region is optically thick enough to completely attenuate the blue side of the line. The damping wing scattering would be effective at wavelengths larger than that corresponds to the blue edge of the H II region, thus the red side of the line would be attenuated by the damping. We used the

damping optical depth as of Loeb, Barkana, & Hernquist (2005). We further assumed the radius of the H II region to be 0.45 proper Mpc (Haiman 2002; Santos 2004). The lower panel of Figure 9 shows the cosmological H II region model fitting to the data, and the best-fit parameters are listed in Table 4. This model also explains fairly well the observed extended red wing. The predicted intrinsic Ly α luminosity from this model is 4.6 times of that of observed, that is roughly consistent with the case of Hu et al. (2002) and its model prediction by Haiman (2002). However, the transmission factor $\sim 20\%$ of the total line flux is smaller than the factor $\sim 50\%$ dimming as suggested by the LF. Here we neglect the possible luminosity dependence of Ly α attenuation, which was suggested by LF seen at § 3. The discrepancy in Ly α attenuation between that supposed by the line profile model fitting and that by the LF difference could be reduced when assuming a larger radius of the H II region. For example, we can obtain $\sim 40\%$ transmission factor when the radius of the H II region to be as large as ~ 0.90 proper Mpc. Although we assume an optically thick core for the H II region, any escape of Ly α flux at the blue side would broaden the line profile, making the fit worse. We can conclude that a larger contribution of the residual neutral hydrogen inside the H II region than the damping wing is required, though our data still lacks the spectral resolution to make quantitative prediction of the density profile inside the H II region.

The fit is better for the galactic wind model; however, our composite spectrum has still too low S/N and spectral resolution to determine which model is more plausible. It should also be noted that there would be a scatter of FWHM among our LAE sample, thus it is unclear whether all of the LAEs have prominent red wings which appeared on the composite spectrum. Whereas in the model, the radiative transfer process of Lyman α photons through emitting galaxy and IGM is too complicated to justify every parameter only by the line profile fitting.

7. IMPLICATIONS TO THE REIONIZATION

In this study, we found that the z6p5LAE LF has a clear deficit at its bright end, compared with that of $z = 5.7$. The simplest interpretation is that the LAE population has some Ly α luminosity evolution from $z = 6.5$ to $z = 5.7$. Strictly speaking, the LAE population has some evolution in EW from $z = 6.5$ to $z = 5.7$, given the result of no evolution of rest UV continuum LF. The LAEs must be very young population having ongoing starburst in so short period that even a hundred million years is a long time, over which their Ly α luminosity can easily drop. Nevertheless, the number density of LAEs does not change from $z \sim 3$ to $z \simeq 5.7$. Thus

it is rather natural to assume that this lack of LF evolution extends up to $z = 6.5$ than assuming that the LAE population happens to have strong evolution between $z = 5.7$ and $z = 6.5$. The number density decline from $z = 5.7$ to $z = 6.5$ could imply a substantial transition of the cosmic ionization state between these epochs. In this section, we offer a possible interpretation of these observational results in relation to the reionization of the universe, assuming that the nature of LAEs themselves has no drastic evolution between $z = 5.7$ and $z = 6.5$.

Assuming a fully ionized IGM at $z = 5.7$, the comparison of the LF between $z = 5.7$ and $z = 6.5$ puts constraints on the neutral fraction of IGM hydrogen $x_{\text{HI}}^{\text{IGM}}$ at $z = 6.5$. The short-dashed and dotted lines in Figure 5 show the Schechter luminosity function, in which the Ly α luminosities are reduced by a factor of 0.6 ($L^* \times 0.6$) and 0.4 from the LF at $z = 5.7$, that is still consistent with our upper and lower limits of LF estimate, respectively. According to the IGM dynamical model of Santos (2004), the Ly α luminosity drop by $\Delta L^* \sim 0.75$ from the fully ionized IGM corresponds to $x_{\text{HI}}^{\text{IGM}} = 0.45$. However this predicted value is strongly model dependent and even the model by Santos (2004) covers a wide range of acceptable models with different predictions of Ly α attenuation. The predicted value of $x_{\text{HI}}^{\text{IGM}}$ could be much smaller than 0.45 in some of these models. Therefore our LF estimate could allow the neutral fraction range of IGM at $z = 6.5$ as $0 \lesssim x_{\text{HI}}^{\text{IGM}} \lesssim 0.45$. This upper limit of $x_{\text{HI}}^{\text{IGM}}$ at $z \sim 6.5$ is in consistent with recent results of Malhotra & Rhoads (2006) and Totani et al. (2006).

Haiman & Cen (2005) evaluated the LF evolution of LAEs taking into account the luminosity dependence of the Ly α flux attenuation. In the epoch of reionization, ionizing sources like LAEs would make cosmological H II regions around them (Miralda-Escude, Haehnelt & Rees 2000). Based on the CDM model, the galaxies embedded in massive dark halos would collapse first, then the ionizing sources in this era would be preferentially located in the high-density regions. The bright LAEs clustered in the overdense region would overlap their H II regions effectively and create a larger H II region with high ionization fractions, which significantly reduces the Ly α flux attenuation. As a result, it is predicted that bright LAEs are readily observed while faint LAEs are more severely attenuated. However this luminosity dependence would just shift the Schechter LF downward by a certain factor according to $x_{\text{HI}}^{\text{IGM}}$ because the LF is steeper at the bright end. Our observed spectroscopic LF (lower estimate) almost agrees with the trend, while our upper limit estimate of the z6p5LAE LF, which has a steep decline at only its bright end, does not agree. Our null result of finding any signals of bright LAE clustering is also inconsistent with the model. As Haiman & Cen (2005) suggested, the predicted LF profile strongly depends on the model assumptions, such as the constant escape fraction with respect to Ly α luminosity.

Assuming a clumpy IGM and discrete ionizing sources, there are two conflicting model predictions about the spatial inhomogeneity of the reionization propagation. In a first phase of reionization, most of the sources are formed in high-density regions and ionize the dense gas around them. If the local neutral IGM around these sources is dense enough to allow higher recombination rates

than ionization rates, the reionization will not complete in these high-density regions. Consequently as in the model prediction by Miralda-Escude, Haehnelt & Rees (2000), H II regions expand preferentially towards low gas density regions, and overdense regions are gradually ionized after the epoch of overlap of cosmological H II regions (“outside-in” model). This picture is supported by hydrodynamic (Gnedin 2000) and N -body (Ciardi, Stoehr, & White 2003) simulations. On the other hand, if the local IGM density is low enough to help an efficient escape of Ly α photons, it is expected that the dense IGM region, in which a large H II region can be formed by overlap of ionized bubbles around high-luminosity sources, is ionized first. It then proceeds to a void where it is dominated by only low-luminosity sources (“inside-out” model). Such a picture is predicted by Sokasian et al. (2003); Furlanetto, Zaldarriaga, & Hernquist (2006b).

The key diverging point between these two models is the IGM density distribution, which Miralda-Escude, Haehnelt & Rees (2000) assume as an extrapolation from that at $z = 3$. However the adequacy of that assumption is still uncertain (Furlanetto, Zaldarriaga, & Hernquist 2006b). These two contradictory models obviously have different predictions about the spatial distribution of observable galaxies in this epoch; galaxies residing in the underdense regions are easily observed in the outside-in model, while galaxies residing in the overdense regions are easily observed in the inside-out model. In turn, a more inhomogeneous galaxy distribution is predicted in the inside-out model. Assuming that we are seeing the final stage of reionization through our observed z6p5LAE sample as deduced from the previous estimation of $0 \lesssim x_{\text{HI}}^{\text{IGM}} \lesssim 0.45$, our observed result of a homogeneous distribution agrees better with the outside-in model. Our assumed picture, in which the LAE overdense regions were still obscured by surrounding thick neutral IGM clouds at $z = 6.5$, is also consistent with our LF deficit for bright LAEs. Such an overdense region could be kept neutral until later epochs, trapping bright ionizing sources like luminous QSOs, in which the appearance of Gunn-Peterson troughs are found at lower- z at $z \sim 5.2 - 5.8$ (Becker et al. 2001; Djorgovski et al. 2001). Inhomogeneous reionization is also suggested by the significant variation in the IGM transmissions among different QSO lines of sights (Djorgovski et al. 2006). In summary, implications to the reionization process suggested by this study are high clumping factor of IGM and inhomogeneous reionization. Although any further quantitative discussions are hardly made, we may be looking at only low-luminosity LAEs residing in low-density IGM regions at the end of the reionization epoch.

We plot in Figure 10 the relation between the local surface number density of LAEs and their Ly α luminosities, $L(\text{Ly}\alpha)$. The local surface number density is measured by the number of LAEs in a circle of $8h_{70}^{-1}$ Mpc comoving radius around each sample object. There is no apparent correlation between the local density and $L(\text{Ly}\alpha)$, suggesting again spatial homogeneity. It should be noted that the local number density in Figure 10 just accounts for our LAE sample, and at this point, there is no way

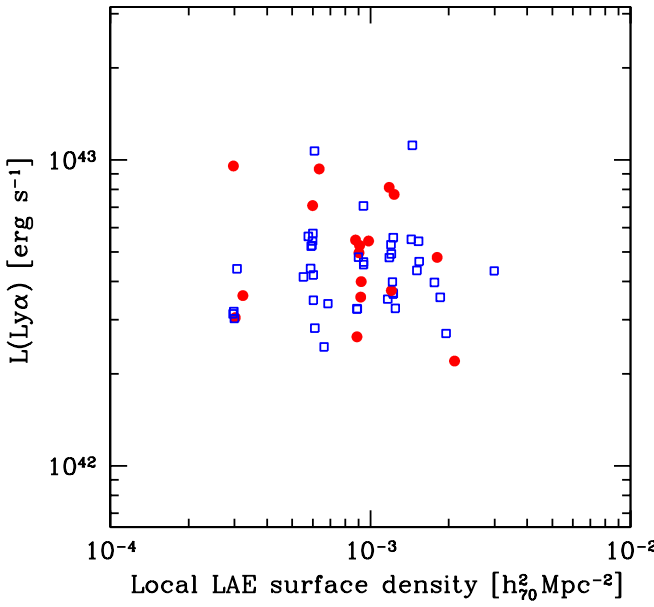


FIG. 10.— Correlation between the Ly α luminosity and the local surface number density for our 58 z6p5LAE sample. The red solid circles are from the spectroscopic sample, while the blue open squares are from the photometric sample.

of inferring the presence of other ionizing sources like i' -drop galaxies without strong Ly α emissions. Nor did we find any clear relation between the local densities and the FWHM of Ly α lines.

Figure 11 shows the FWHM of Ly α emissions as a function of $L(\text{Ly}\alpha)$ for our spectroscopic z6p5LAE sample. There is a weak anti-correlation between FWHM and $L(\text{Ly}\alpha)$. Haiman & Cen (2005) predicted a similar correlation, which they proposed as an independent diagnostic of $x_{\text{HI}}^{\text{IGM}}$, aside from the LF. The blue side of Ly α emission is dominantly attenuated by the residual H I inside the cosmic H II regions. A systematic high velocity, as in galactic winds, would reduce more effectively the amount of residual H I for smaller H II regions surrounding low-luminosity sources: thus the anti-correlation is expected. This effect would depend more sensitively on the line width at the blue side, which is, however, difficult to measure precisely. The correlation is expected to be steeper for higher $x_{\text{HI}}^{\text{IGM}}$; however the observed correlation in Figure 11 shows too much scatter to determine $x_{\text{HI}}^{\text{IGM}}$. The observed anti-correlation could be a sign of a high $x_{\text{HI}}^{\text{IGM}}$ indicating that cosmic reionization has not been completed at $z = 6.5$. A possible variation of systematic internal velocity among LAEs would also dilute the relation. The intrinsic relation between FWHM and $L(\text{Ly}\alpha)$ has been not clearly established. Matsuda (2005) found a clear positive correlation between the velocity dispersion and $L(\text{Ly}\alpha)$ for their large Ly α blob sample at $z \sim 3$ in the SSA22 proto-cluster region. The intrinsic relation should be determined for the general LAE populations

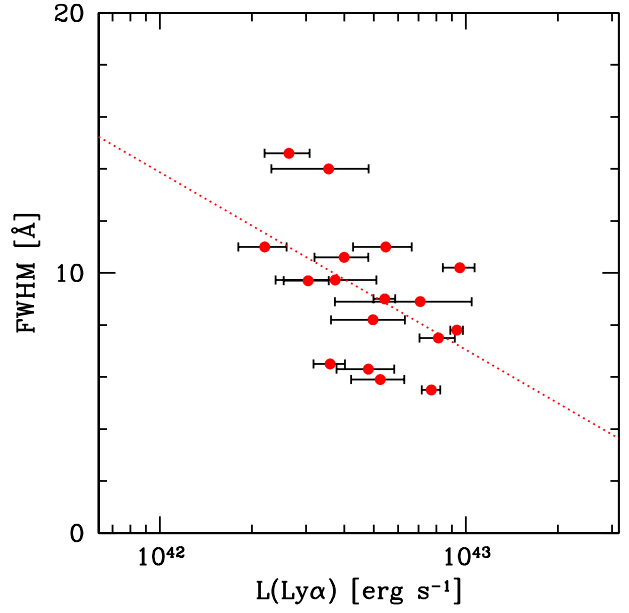


FIG. 11.— Correlations between the Ly α luminosity and the FWHM of the Ly α emission line for our sample of 17 spectroscopically confirmed z6p5LAEs. The dotted line is the fiducial linear fit.

at lower- z where it is irrelevant to the reionization.

The possible implications for the reionization described above are still speculative because there are many unknown factors. First, we did not take into account the inherent galactic evolution of LAEs. It is suggested by previous studies that the number density of LAEs between $z = 3$ and $z = 6$ is almost unchanged, which is in contrast to the LBG population with significant LF evolution from $z = 3$ to $z = 6$ (Ouchi et al. 2004; Bouwens et al. 2005; Yoshida et al. 2006). However less than 20 LAEs have been confirmed spectroscopically even at $z \sim 3$, not enough to determine accurately the LF. On the other hand, Bouwens et al. (2005) have found an evidence for evolution of the rest-frame continuum UV LF between $z \sim 3$ and $z \sim 6$. Also, there is no consensus on the spatial distribution of LAE at low redshifts. They might have an intrinsically homogeneous distribution. The inherent evolutions of Ly α flux, dust content, and neutral gas fraction inside LAEs themselves would also decrease the number density from $z = 5.7$ to $z = 6.5$. The complex escape mechanism of ionizing radiation from galaxies is unclear, and depends closely on assumed parameters such as the escape fraction of Ly α photons, amount of dust, galactic wind, and star formation activity. Our observed z6p5LAE LF could be more consistent with the quiescent hierarchical model prediction by Le Delliou et al. (2005) than with their model including an on-going starburst. And finally, we do not know completely about the IGM physical condition during the reionization epoch, and no observational evidence

has been found for the cosmological H II region which is fundamentally predicted by today's reionization models. Although there are many ingredients to be considered, our conjecture can be plausible to give a reasonable explanation to our results.

8. CONCLUSIONS

We carried out spectroscopic observations with Subaru and Keck to identify z6p5LAEs that are selected by narrow-band excess at $\sim 920\text{nm}$, and our conclusions can be summarized as follows:

1. We have identified eight new z6p5LAEs based on their significantly asymmetric Ly α emission profiles, to increase the sample of spectroscopically confirmed $z = 6.5$ LAEs in the Subaru Deep Field to 17.

2. We have constructed a large homogeneous spectroscopic sample from the photometric sample of 58 LAE candidates, to determine the Ly α LF at $z = 6.5$. The LF reveals an apparent deficit at least at the bright end, compared with that of $z = 5.7$. The L^* difference between $z = 6.5$ and $z = 5.7$ is ~ 0.75 mag for fixed $\alpha = -1.5$. The difference has 3σ significance, which reduces to 2σ when we take into account the cosmic variance. There could also be a decrease of comoving number density of LAEs from $z = 5.7$ to $z = 6.5$ at the faint end, although the conclusion could be modified by further follow-up spectroscopy.

3. The rest UV continuum LF of our LAE sample at $z = 6.5$ has almost the same as those of LAE sample at $z = 5.7$ and i-dropout sample at $z \sim 6$, even at their bright ends.

4. The spatial distribution of z6p5LAEs was found to be homogeneous over the field, based on three independent methods to quantify the clustering strength. We cannot deny the possibility that we happen to see a very homogeneous region of the $z = 6.5$ universe.

5. The composite spectrum of 12 z6p5LAE sample with high spectral resolution clearly reveals an asymmetric Ly α profile with an extended red wing. The profile can be explained by either the galactic wind model composed of double Gaussian profiles, or by the reionization model expected for a typical profile during the reionization epoch.

6. The observed results could imply that the reionization of the universe has not been completed at $z = 6.5$. The decline of the z6p5LAE LF could imply $0 \lesssim x_{\text{HI}}^{\text{IGM}} \lesssim 0.45$ based on the IGM dynamical model of Santos (2004). A conjecture that we are seeing the final stage of reionization at $z = 6.5$, when the LAE over-

dense regions were still obscured by thick neutral IGM clouds around them, qualitatively agrees with our results of deficient bright LAEs and their homogeneous spatial distribution.

Our z6p5LAE spectroscopic sample is not yet large enough to make a more precise comparison with LFs at lower redshifts. At the moment, it is not clear whether the true LF of z6p5LAE is closer to our upper limit estimate or lower. Thus it is not concluded which differences in L^* and ϕ^* dominate in the disagreement of LF between $z = 6.5$ and $z = 5.7$. In this study, we could not constrain α , the faint end slope of LF. The faint end of the z6p5LAE sample would critically determine the LAE contribution as ionizing sources to the photon budget of the cosmic reionization. Even if the number density of LAEs is low, a significant number of another star-forming population, LBGs, if they exist at this high- z epoch, could complete the reionization. Alternatively, only a small number of galaxies with huge star formation rates at very high redshift can reionize the universe (Panagia et al. 2005; Mobasher et al. 2005). It is too difficult to sample LBGs at exactly the same redshift of LAEs, whereas it is not certain what fraction of LBGs at this epoch shows strong enough Lyman alpha emission to be observed as LAEs. The evolutionary connection between LBGs and LAEs are linked to this problem. Shimasaku et al. (2006) found from the rest UV luminosity LF of the $z = 5.7$ LAE sample that $\sim 80\%$ or more of the LBG population would have strong Ly α emission at $z \sim 6$. This study shows that the rest UV luminosity LF at $z = 6.5$ agree with that of $z = 5.7$, suggesting the same high fraction. The faint end of the LF of z6p5LAE may barely be determined with the spectroscopic capability of today's 8m-telescopes. Nevertheless, steady efforts of further spectroscopic confirmation are certainly required for z6p5LAEs.

We are grateful to the Keck Observatory staff for their help with the observation. We deeply appreciate the devoted technical and management support of the Subaru Telescope staff for this long-term project. The observing time for part of this project was committed to all the Subaru Telescope builders. We thank the referee for helpful comments that improved the manuscript. The research is supported by the Japan Society for the Promotion of Science through Grant-in-Aid for Scientific Research 16740118.

REFERENCES

Ajiki, M., et al. 2003, AJ, 126, 2091
 Barkana, R., & Loeb, A. 2004, ApJ, 609, 474
 Becker, R.H. et al. 2001, AJ, 122, 2850
 Bouwens, R.J. et al. 2003, ApJ, 595, 589
 Bouwens, R.J. et al. 2005 astro-ph/0509641
 Bunker, A., Stanway, E., Ellis, R., McMahon, R., Eyles, L., & Lacy, M. 2006, NewAR, 50, 94
 Ciardi, B., Stoehr, F., & White, S.D.M. 2003, MNRAS, 343, 1101
 Cowie, L. & Hu, E. 1998, AJ, 115, 1319
 Croton, D.J. et al. 2004, MNRAS, 352, 828
 Cuby, J.G., Le Fevre, O., McCracken, H., Cuillandre, J.C., Magnier, E., & Meneux, B. 2003, A&A, 405, L19
 Dawson, S., Spinrad, H., Stern, D., Dey, A., van Breugel, W., de Vries, W., Reuland, M. 2002, ApJ, 570, 92
 Djorgovski, S.G., Castro, S., Stern, D., Mahabal, A. A. 2001, ApJ, 560, L5
 Djorgovski, S.G., Bogosavljevic, M. & Mahabal, A., 2006, NewAR, 50, 140
 Dickinson, M. et al. 2004, ApJ, 600, L99
 Ellis, R., Santos, M.R., Kneib, J.P., & Kuijken, K. 2001, 560, L119
 Faber, S. et al. 2003, Proc. SPIE, 4841, 1657
 Fan, X., Narayanan, V.K., Strauss, M.A., White, R.L., Becker, R.H., Pentericci, L., Rix, H.-W. 2002, AJ, 123, 1247
 Furlanetto, S.R., & Oh, S.P. 2005, MNRAS, 363, 1031
 Furlanetto, S.R., McQuinn, M. & Hernquist, L. 2005, MNRAS, 365, 115
 Furlanetto, S.R., Zaldarriaga, M., & Hernquist, L. 2006, MNRAS, 365, 1012
 Gnedin, N.Y. 2000, ApJ, 535, 530

Haiman, Z. & Spaans, M. 1999, ApJ, 518, 138
 Haiman, Z., 2002, ApJ, 576, L1
 Haiman, Z. & Cen, R. 2005, ApJ, 623, 627
 Hu, E.M., Cowie, L.L., McMahon, R.G., Capak, P., Iwamuro, F., Kneib, J.-P., Maihara, T., Motohara, K. 2002, ApJ, 568, L75; Erratum, 576, L99
 Hu, E.M., Cowie, L.L., Capak, P., McMahon, R.G., Hayashino, T., Komiyama, Y. 2004, AJ, 127, 563
 Kashikawa, N. et al. 2002, PASJ, 54, 819
 Kashikawa, N. et al. 2004, PASJ, 56, 1011
 Kashikawa, N. et al. 2006, ApJ, 637, 631
 Kneib, J.-P., Ellis, R.S., Santos, M.R., Richard, J. 2004, ApJ, 607, 697
 Kodaira, K. et al. 2003, PASJ, 55, L17
 Kudritzki, R.P. et al. 2000, ApJ, 536, 19
 Kurk, J.D., Cimatti, A., di Serego Alighieri, S., Vernet, J., Daddi, E., Ferrara, A., Ciardi, B. 2004, A&A, 422, L13
 Kunth, D., Mas-Hesse, J.M., Terlevich, E., Terlevich, R., Lequeux, J., Fall, S. M. 1998, A&A, 334, 11
 Landy, S.D., & Szalay, A.S. 1993, ApJ, 412, 64
 Le Delliou, M., Lacey, C., Baugh, C.M., Guiderdoni, B., Bacon, R., Courtois, H., Soubie, T., Morris, S.L. 2005, MNRAS, 357, L11
 Loeb, A., Barkana, R. & Hernquist, L. 2005, ApJ, 620, 553
 Ly, C. et al. 2006, submitted to APJ
 Maier, C. et al. 2003, A&A, 402, 79
 Malhotra, S. & Rhoads, J.E. 2004, ApJ, 617, L5
 Malhotra, S. et al., 2005, ApJ, 626, 666
 Malhotra, S. & Rhoads, J.E. 2006, astro-ph/0511196
 Martin, C.L., Sawicki, M., Dressler, A., & McCarthy, P.J., 2006, NewAR, 50, 53
 Mas-Hesse, J.M., Kunth, D., Tenorio-Tagle, G., Leitherer, C., Terlevich, R. J., Terlevich, E. 2003, ApJ, 598, 858
 Matsuda, Y. 2005, PhD thesis, Tohoku University.
 Miralda-Escude, J. & Rees, M.J., 1998, ApJ, 497, 21
 Miralda-Escude, J., Haehnelt, M. & Rees, M.J., 2000, ApJ, 530, 1
 Mobasher, B. et al. 2005, ApJ, 635, 832
 Nagao, T. et al. 2004, ApJ, 613, L9
 Nagao, T. et al. 2005, ApJ, 634, 142
 Ouchi, M. et al., 2004, ApJ, 611, 660
 Ouchi et al., 2005, ApJ, 620, L1
 Page et al., 2006, astro-ph/0603450
 Palunas, P., Teplitz, H.I., Francis, P.J., Williger, G.M., & Woodgate, B.E. 2004, ApJ, 602, 545
 Panagia, N. et al., 2005, ApJ, 633, L1
 Peacock, J.A. 1983, MNRAS, 202, 615
 Pelló, R., Schaerer, D., Richard, J., Le Borgne, J.-F., Kneib, J.-P. 2004, A&A, 416, L35
 Pettini, M., Rix, S.A., Steidel, C.C., Adelberger, K.L., Hunt, M.P., Shapley, A.E. 2002, ApJ, 569, 742
 Rhoads, J.E. & Malhotra, S. 2001, ApJ, 563, L5
 Rhoads, J.E. et al. 2003, AJ, 125, 1006
 Rhoads, J.E. et al. 2004, ApJ, 611, 59
 Santos, M.R. 2004, MNRAS, 349, 1137
 Shapley, A.E., Steidel, C.C., Pettini, M., Adelberger, K.L. 2003, ApJ, 588, 65
 Shimasaku, K. et al. 2003, ApJ, 586, L111
 Shimasaku, K. et al. 2004, ApJ, 605, L93
 Shimasaku, K. et al. 2006, PASJ in press, astro-ph/0602614
 Sokasian, A., Abel, T., Hernquist, L., Springel, V. 2003, MNRAS, 344, 607
 Somerville, R.S., Lee, K., Ferguson, H.C., Gardner, J.P., Moustakas, L.A., Giavalisco, M. 2004, ApJ, 600, L171
 Spergel, D.N. et al. 2006, astro-ph/0603449
 Stanway, E.R., McMahon, R.G. & Bunker, A.J. 2005, MNRAS, 359, 1184
 Steidel, C.C., Adelberger, K.L., Shapley, A.E., Pettini, M., Dickinson, M., Giavalisco, M. 2000, ApJ, 532, 170
 Stern, D., Yost, S.A., Eckart, M.E., Harrison, F.A., Helfand, D.J., Djorgovski, S.G., Malhotra, S., Rhoads, J.E. 2005, ApJ, 619, 12
 Stiavelli, M. et al., 2005, ApJ, 622, L1
 Taniguchi, Y. et al. 2005, PASJ, 57, 165 (T05)
 Totani, T., Kawai N., Kosugi G., Aoki K., Yamada T., Iye M., Ohta K., & Hattori T. 2006, PASJ in press astro-ph/0512145
 Tran, K.-V.H., Lilly, S.J., Crampton, D., Brodwin, M. 2004, ApJ, 612, L89
 van Breukelen, C., Jarvis, M.J., & Venemans, B.P., 2005, MNRAS, 359, 895
 Westra, E., Jones, D.H., Lidman, C.E., Athreya, R.M., Meisenheimer, K., Wolf, C., Szeifert, T., Pompei, E., Vanzi, L. 2005, A&A, 430, L21
 White, S.D.M. 1979, MNRAS, 186, 145
 Willott, C.J et al., 2005, ApJ, 633, 630
 Wyithe, J.S.B., & Loeb, A., 2004, Nature, 432, 194
 Wyithe, J.S.B., & Loeb, A., 2005, ApJ, 625, 1
 Yan, H. & Windhorst, R.A., 2004, ApJ, 600, 1
 Yoshida, M., et al. 2006, submitted to APJ

APPENDIX

SKEWNESS: THE ASYMMETRY INDICATOR OF HIGH- Z LY α EMISSION LINE

We describe here a statistic *skewness* S to measure the asymmetry of high- z Ly α emission lines. This model-independent indicator is free from fitting procedures that sometimes require smoothing of noisy spectra.

The S is a popular statistic defined as the 3rd moment of the distribution function to see its asymmetry (see also Kurk et al. 2004). Here we regard the observed spectrum, which is basically a 2-dimensional array of the flux (f_i) and the pixel (x_i), as a distribution function with an array size of n . S is defined as,

$$S = \frac{1}{I\sigma^3} \sum_i^n (x_i - \bar{x})^3 f_i, \quad (\text{A1})$$

where $I = \sum_i^n f_i$, \bar{x} and σ are the average and dispersion of x_i defined as,

$$\bar{x} = \frac{1}{I} \sum_i^n x_i f_i, \quad (\text{A2})$$

and

$$\sigma^2 = \frac{1}{I} \sum_i^n (x_i - \bar{x})^2 f_i, \quad (\text{A3})$$

respectively.

This statistic is free from fitting procedures such as the a_λ and a_f presented by Rhoads et al. (2003). Their asymmetry estimation is based on two-component Gaussian profile fitting for the red and blue sides of the emission. However it is sometimes too difficult to determine of line peak wavelength λ_p or λ_{10} where the flux drops to 10% of its peak value that strongly depend on the resolving power and quality of the data.

We now estimate the error of S , which can be analytically derived. We here assume $\delta x_i \sim 0$, and approximately regard the 1st-order derivative of skewness as its error.

$$\delta S = \left(\sum_i^n \left(\frac{\partial S}{\partial f_i} \delta f_i \right)^2 \right)^{0.5} = \frac{1}{I} \left(\sum_i^n \left[\left(\frac{x_i - \bar{x}}{\sigma} \right)^3 - \frac{3S}{2} \left(\frac{x_i - \bar{x}}{\sigma} \right)^2 - 3 \left(\frac{x_i - \bar{x}}{\sigma} \right) + \frac{S}{2} \right]^2 \delta f_i^2 \right)^{0.5}, \quad (\text{A4})$$

where we use

$$\frac{\partial \bar{x}}{\partial f_i} = \frac{1}{I} (x_i - \bar{x}), \quad (\text{A5})$$

and

$$\frac{\partial \sigma}{\partial f_i} = \frac{1}{2\sigma I} \{ (x_i - \bar{x})^2 - \sigma^2 \}. \quad (\text{A6})$$

We can assume that the flux error does not strongly depend upon the wavelength as in the case of our narrow-band filter coverage where is the night sky window almost free from OH emission lines. Under the assumption, the δf_i can be then regarded as $\delta f_i \sim \delta f = \text{const.}$ dominated by readout noise around the emission line on the spectrum.

This error estimate is confirmed to agree well with the rms fluctuation of S evaluated by a Monte Carlo realization, in which line profile model is disturbed with random artificial errors as large as δf . Our estimate of skewness error in (A4) gives a useful analytic formula, though more strict error estimate should be directly achieved with such a Monte Carlo simulation.

We compare this statistic S with a_λ proposed by Rhoads et al. (2003) for our $NB921$ -excess sample in Figure A12. We here calculate S in the effective wavelength range of an emission line where f_i have apparent positive signals above the continuum (sky) level. The slight change of the effective wavelength range does not significantly affect the result. Foreground emitters shown in Figure A12 are definitely identified by their multiple lines on spectra. That is, an H α emitter has corresponding [O III] doublets around 7016Å, and [O III] and [O II] emitters show apparent doubles by themselves (and sometimes H β for the [O III] case). As expected, [O II], [O III], and H α emitters distribute around $S = 0$ and $a_w = 1$. The resolved [O II] doublet lines are expected to be show negative S because $\lambda 3726$ is typically weaker than $\lambda 3729$. There is a population (red circles) that have actually larger positive S and a_w , indicating statistically asymmetric lines with broad red wing. We recognize them as Ly α emitters that have $S > 0.15$. Almost all the single line emitters (yellow triangles) show relatively low S which indicates that they are likely to be [O II] emitters. The large scatter of S for these single line emitters was caused by low signal-to-noise ratio of their spectra.

